Original Article

MOLECULAR METABOLISM

Cyp2c-deficiency depletes muricholic acids and protects against high-fat diet-induced obesity in male mice but promotes liver damage

Antwi-Boasiako Oteng [1,2], Sei Higuchi [1,2], Alexander S. Banks [3], Rebecca A. Haeusler [1,2,*]

ABSTRACT

Objective: Murine-specific muricholic acids (MCAs) are reported to protect against obesity and associated metabolic disorders. However, the response of mice with genetic depletion of MCA to an obesogenic diet has not been evaluated. We used Cyp2c-deficient ($Cyp2c^{-/-}$) mice, which lack MCAs and thus have a human-like bile acid (BA) profile, to directly investigate the potential role of MCAs in diet-induced obesity.

Methods: Male and female $Cyp2c^{-/-}$ mice and wild-type (WT) littermate controls were fed a standard chow diet or a high-fat diet (HFD) for 18 weeks. We measured BA composition from a pool of liver, gallbladder, and intestine, as well as weekly body weight, food intake, lean and fat mass, systemic glucose homeostasis, energy expenditure, intestinal lipid absorption, fecal lipid, and energy content.

Results: Cyp2c-deficiency depleted MCAs and caused other changes in BA composition, namely a decrease in the ratio of 12α-hydroxylated (12α-OH) BAs to non-12α-OH BAs, without altering the total BA levels. While WT male mice became obese after HFD feeding, $Cyp2c^{-/-}$ male mice were protected from obesity and associated metabolic dysfunctions. $Cyp2c^{-/-}$ male mice also showed reduced intestinal lipid absorption and increased lipid excretion, which was reversed by oral gavage with the 12α-OH BA and taurocholic acid (TCA). $Cyp2c^{-/-}$ mice also showed increased liver damage, which appeared stronger in females.

Conclusions: MCA does not protect against diet-induced obesity but may protect against liver injury. Reduced lipid absorption in Cyp2c-deficient male mice is potentially due to a reduced ratio of 12α-OH/non-12α-OH BAs.

Keywords Bile acid; Muricholic acid; Obesity; Lipid absorption; Glucose homeostasis; Liver fibrosis

1. INTRODUCTION

Bile acids (BAs) are catabolites of cholesterol that are synthesized in the liver and secreted into the gut. Liver-derived primary BAs are exported as glycine or taurine conjugates, the former most prominent in humans and the latter most prominent in mice, and can be converted to unconjugated and secondary BAs in the gut by resident microbes [1,2]. In the gut, BAs facilitate the absorption of fats, cholesterol, and fat-soluble vitamins. BAs also possess endocrine functions by serving as ligands for the transcription factor farnesoid X receptor (FXR) and Takeda G protein-coupled receptor 5 (TGR5), thus enabling BAs to play important roles in the physiological regulation of lipid and glucose metabolism [3–5].

Human studies have shown that BA levels, composition, and signaling are associated with cardiometabolic diseases such as obesity, dyslipidemia, and diabetes [6], highlighting the potential of BA modulation in treating or preventing such disorders. Obesity in humans is positively associated with increased synthesis of BA, impaired serum BA fluctuations, and increased synthesis of 12α-hydroxylated BAs, which include cholic acid (CA) and its secondary BA derivative deoxycholic acid (DCA) [7]. Additionally, the ratio of 12α-hydroxylated to non-12α-hydroxylated BAs is positively correlated with human insulin resistance [8]. To establish whether alterations of BA metabolism play a causal role in cardiometabolic disorders, mechanistic studies in preclinical models are important. Many such mechanistic investigations have been conducted in rats and mice. However, the use of these models is translationally challenging, because mice produce muricholic acids (MCAs) that are not present in healthy adult humans.

MCAs are trihydroxylated at carbons 3, 6, and 7, and their unique structures are thought to cause differential functionality. For one thing,

[1]Naomi Berrie Diabetes Center, Columbia University Medical Center, New York, NY, USA [2]Department of Pathology and Cell Biology, Columbia University Medical Center, New York, NY, USA [3]Division of Endocrinology, Beth Israel Deaconess Medical Center and Harvard Medical School, Boston, MA, USA

*Corresponding author. Naomi Berrie Diabetes Center, Columbia University Medical Center, Russ Berrie Pavilion, 1150 St Nicholas Avenue, New York, NY, 10032, USA. E-mail: rah2130@cumc.columbia.edu (R.A. Haeusler).

Abbreviations: 12, α-OH BA; 12, α-hydroxylated bile acid; ALT, alanine transaminase; AST, aspartate transaminase; BA, bile acid; CA, cholic acid; CDCA, chenodeoxycholic acid; CM, chylomicron; Cyp2c, Cytochrome P450 2C; Cyp7a1, cytochrome P450, family 7, subfamily a, polypeptide 1; Cyp7b1, cytochrome P450, family 7, subfamily b, polypeptide 1; Cyp8b1, cytochrome P450, family 8, subfamily b, polypeptide 1; Cyp27a1, cytochrome P450, family 27, subfamily a, polypeptide 1; DCA, deoxycholic acid; FXR, farnesoid X receptor; HDL, high-density lipoprotein; HDCA, hyodeoxycholic acid; LCA, lithocholic acid; LDL, low-density lipoprotein; MCA, muricholic acid; SHP, small heterodimer partner; TCA, taurocholic acid; UDCA, ursodeoxycholic acid; VLDL, very low-density lipoprotein

Received May 23, 2021 • Revision received August 8, 2021 • Accepted August 18, 2021 • Available online 24 August 2021

https://doi.org/10.1016/j.molmet.2021.101326

some MCAs can antagonize, rather than activate, FXR [9–11]. Furthermore, MCAs are thought to be poor at promoting fat and cholesterol absorption. This concept is supported by studies that used dietary interventions to increase MCAs in mice, which results in reduced cholesterol absorption [12]. Other studies have indirectly increased MCAs by deleting the 12α-hydroxylase Cyp8b1, thus eliminating the 12α-hydroxylated BAs such as CA and DCA, and increasing the non-12α-hydroxylated BAs (which, in mice, are primarily MCAs). This results in reduced absorption of dietary fat and cholesterol, lower body weight, and protection against diet-induced obesity [13–17]. Thus, it has been suggested that MCAs play a causal role in protection against weight gain and diet-induced obesity. However, the direct effects of MCAs on obesity and associated metabolic disorders have not been evaluated in a mouse model with specific genetic elimination of MCAs.

An insightful study by Takahashi et al. [18] demonstrated that the presence of MCAs in mice requires the *Cyp2c* cluster of genes, which includes 14 gene isoforms. Recent studies show that specifically deleting *Cyp2c70* reduces MCAs and causes a concomitant increase in chenodeoxycholic acid (CDCA), which is the major precursor BA for MCA synthesis [19–21]. To determine the effects of eliminating MCAs on fat absorption and susceptibility to obesity and its associated metabolic complications, we used mice with a germline deletion of the 14 Cyp2c isoforms that are clustered on mouse chromosome 19 ($Cyp2c^{-/-}$) [22,23]. BA analysis confirmed the lack of MCAs, and one might predict this to enhance intestinal lipid absorption and increase susceptibility to diet-induced obesity. On the other hand, $Cyp2c^{-/-}$ mice also showed a significant reduction in levels of 12α-OH BAs compared to control mice. Because 12α-OH BAs promote fat absorption [14,16], this suggests the opposing possibility that $Cyp2c^{-/-}$ mice would be less susceptible to diet-induced obesity. To distinguish between these possibilities, we set out to investigate the response to an obesogenic diet by $Cyp2c^{-/-}$ mice.

2. MATERIALS & METHODS

2.1. Animal model and interventions

2.1.1. Generation and source of $Cyp2c^{-/-}$ mice

Animal experiments were conducted in wild-type (WT) and Cyp2c-knockout ($Cyp2c^{-/-}$) mice with C57BL/6 N background obtained from Taconic Biosciences (New York, NY, USA). The mice (model # 9177) were originally generated by a Cre-mediated germline deletion of 14 out of 15 isoforms of the Cyp2c genes. The deleted genes, which are located within a 1.2 Mb cluster on chromosome 19, include *Cyp2c55*, *2c65*, *2c66*, *2c29*, *2c38*, *2c39*, *2c67*, *2c68*, *2c40*, *2c69*, *2c37*, *2c54*, *2c50*, and *2c70*. *Cyp2c44*, which is physically located outside of this cluster, has not been deleted. The resultant chimeras were backcrossed to C57BL/6 N WT mice [22]. Male and female heterozygotes were subsequently purchased from Taconic Biosciences and bred to generate knockout mice and littermate controls for this study. Mice were genotyped using a genotyping kit (#KK5621, KAPA Biosystems). The DNA products after PCR were resolved by electrophoresis on a 2% agarose gel with 0.05% ethidium bromide. The primer sequences used for genotyping are provided in Supplemental Table 1.

2.1.2. Chow, high-fat diet (HFD), and western diet intervention

Male WT (n = 7), male $Cyp2c^{-/-}$ (n = 7), female WT (n = 7), and female $Cyp2c^{-/-}$ (n = 7) mice were weaned onto and maintained on standard chow diet (3.4 kcal/g, Purina 5053, 24.7% kcal from protein, 62.1% carbohydrate, and 13.2% fat) *ad libitum*. Body weights were measured once every week until mice were euthanized at ∼30 weeks old. When mice were between 17 and 20 weeks old, oral glucose tolerance tests (OGTT) and insulin tolerance tests (ITT) were performed.

During the HFD intervention, male WT (n = 7), male $Cyp2c^{-/-}$ (n = 7), female WT (n = 5), and female $Cyp2c^{-/-}$ (n = 5) mice were weaned onto standard chow diet until mice were transferred onto a HFD (60% kcal fat, D12492, Research Diets Inc., New Brunswick, NJ, USA) at 7–8 weeks old. The mice were fed the HFD for 18 weeks. Body weights were measured once every week. OGTT and ITT were performed after 12 and 14 weeks on the HFD, respectively.

During the western diet intervention, male WT (n = 8), male $Cyp2c^{-/-}$ (n = 8), female WT (n = 7), and female $Cyp2c^{-/-}$ (n = 7) mice were weaned onto standard chow diet until mice were transferred onto a western diet (4.5 kcal/g, 42% kcal from fat and 0.2% from cholesterol, TD 88137: Envigo) at 7–8 weeks old. The mice were fed the western diet for 10 weeks. Body weights were measured once every week. OGTT and ITT were performed after 6 and 7 weeks on the western diet, respectively.

In all groups, mice were singly housed two weeks prior to euthanasia to collect feces and to measure food intake using feeding dispensers that were placed inside the cage. One week before euthanasia, mice were subjected to a body composition assessment for lean and fat mass using time-domain NMR (Minispec Analyst AD; Bruker Optics) [24] followed by indirect calorimetry in male mice on chow and HFD using metabolic cages for energy expenditure measurement.

Mice were euthanized using CO_2 asphyxiation followed by cervical dislocation. Blood was collected through the inferior vena cava into EDTA-coated tubes to obtain plasma followed by excision of liver, gonadal white adipose tissue (gWAT), brown adipose tissue (BAT), and intestine for analysis.

All experiments were approved by and conducted in accordance with the guidelines of the Columbia University Institutional Animal Care and Use Committee.

2.1.3. Glucose tolerance test (GTT)

Following a 6-hour fast, baseline glucose measurements representing timepoint 0 were recorded via tail vein bleeding using OneTouch glucose monitor and strips (LifeScan). Mice were then orally gavaged (in case of OGTT) or injected intraperitoneally (in case of IPGTT) with glucose (2 g/kg of body weight) followed by glucose measurements at timepoints 15, 30, 60, 90, and 120 min.

2.1.4. Insulin tolerance test (ITT)

Following a 5-hour fast, baseline glucose measurements representing timepoint 0 were recorded via tail vein bleeding using OneTouch glucose monitor and strips (LifeScan). Mice were then injected intraperitoneally with insulin (0.5U/kg body weight) followed by glucose measurements at timepoints 15, 30, 45, and 60 min.

2.1.5. Metabolic cages

Indirect calorimetry measurements were performed with Comprehensive Laboratory Animal Monitoring System (CLAMS) and open-circuit Oxymax system (Columbus Instruments). Mice were individually housed for 7 days in metabolic cages. The animals were housed at 22 °C for the duration of the measurements with a 07:00–19:00 light photoperiod. Mice were aged 26–29 weeks and 24–25 weeks for experiments on chow or HFD, respectively. The analysis of energy expenditure was performed using CalR [25]. In cages where hoppers

malfunctioned and did not register food intake for 36 h, mice were excluded from the analyses. Final n used for analyses are reported in the figure legends.

2.1.6. Fasting Re-feeding experiment

Mice maintained on chow diet were fasted overnight, and re-fed for 2 h with HFD. Blood was collected after fasting and after re-feeding and centrifuged at 2,500 g for 15 min to obtain plasma.

2.1.7. Taurocholic acid (TCA) gavage experiment

Mice were orally gavaged with 17 mg/kg TCA in 1.5% $NaHCO_3$ at 6 pm each day for 3 consecutive days. The 17 mg/kg dose was chosen based on earlier publications demonstrating that a dose in this range has does not alter the total BA levels but raises the TCA levels in mice [26,27]. On day 4, mice underwent the radiolabeled triolein experiment to measure lipid absorption.

2.1.8. Radiolabeled triolein experiment

For analysis of lipid absorption, mice maintained on chow diet underwent a 4-hour fast between 7 am and 11 am, injected intraperitoneally with poloxamer 407 (1 g/kg body weight) in PBS [28], then orally gavaged with olive oil (10 μL/g body weight) containing 2.5 μCi of [^{3}H]triolein ([9—10-3 H(N)]triolein; PerkinElmer), which is a radiolabeled triglyceride. Mice were bled before the gavage at time 0, and then at 1, 2, 4, 8, and 24-hours post-gavage. Blood samples were analyzed for radioactivity (Tricarb 2910 TR Scintillation Counter; PerkinElmer).

2.1.9. Liver acylglycerol secretion

To assess changes in liver VLDL-triglyceride secretion, we fasted male mice for 6 h and collected plasma at timepoint 0, followed immediately by injection of poloxamer 407 (1 g/kg body weight) in PBS [28]. Plasma was then collected 1, 2, and 4 h after poloxamer 407 injection, and acylglycerols were measured.

2.2. Bile acid (BA) profile

The liver, gallbladder, and small intestine were doubly homogenized in 50% methanol using a rotor-stator homogenizer, followed by a Dounce Teflon glass homogenizer. Deuterated BA standard (20 μL of 25 μM d4-cholic acid) was added to 200 μL of each sample, and calibrator curves were generated of each BA in charcoal-stripped tissue. To each sample/calibrator, 2 mL of ice-cold acetonitrile was added, then samples were vortexed for 1 h at 2,000 rpm and centrifuged for 10 min at 11,000 g. Supernatants were transferred to clean glass tube and dried down at 45 °C under nitrogen. Each sample/calibrator was extracted a second time in 1 mL of ice-cold acetonitrile, vortexed for 1 h at 2,000 rpm, and centrifuged for 10 min at 11,000 g. The supernatant of the second extraction was combined with the first and dried down at 45 °C under nitrogen. Each sample was resuspended in 200 μL of 55:45 (vol/vol) methanol:water, both with 5 mM ammonium formate. Samples were centrifuged in UltraFree MC 0.2-μm centrifugal filters (Millipore) and transferred to liquid chromatography-mass spectrometry (LC-MS) vials, and 10 μL were injected into ultraperformance liquid chromatography-tandem mass spectrometry vials (UPLC-MS/MS; waters).

2.3. Plasma analysis

Blood glucose was measured in mice that were fasted for 5 h by tail vein bleeding using OneTouch glucose monitor and strips (LifeScan). Plasma was obtained after centrifuging blood collected in EDTA-coated tubes for 15 min at 2,500 g. Plasma insulin was measured using an ELISA kit (# 10-1247-01, Mercodia) according to the manufacturer's protocol. Plasma lipids were measured using colorimetric assays for triglycerides (Infinity; Thermo Scientific), non-esterified fatty acids (NEFA) (Wako Diagnostics), and cholesterol (Cholesterol E, Wako Diagnostics). Plasma alanine aminotransferase (ALT) (MAK052, Sigma) and aspartate aminotransferase (AST) (MAK055, Sigma) were measured using dedicated kits according to the manufacturer's protocol.

2.4. Plasma lipoprotein analysis by fast protein liquid chromatography (FPLC)

Plasma lipoproteins were analyzed by running 200 μL of pooled plasma onto an FPLC system consisting of 2 Superose 6 columns connected in series (Amersham Pharmacia Biotech) as described previously [29].

2.5. Histology

2.5.1. Hematoxylin & eosin staining

This was performed on formalin-fixed liver, perigonadal white adipose tissue (pgWAT), and BAT. Tissues were processed using ethanol and xylene before being embedded into paraffin blocks. Liver sections of 5 μm thickness were made using a microtome onto Superfrost glass slides and incubated at 37 °C overnight. Tissue slices were then stained for 10 min in Mayer hematoxylin solution and for 10 s in eosin Y solution. The slides were then observed under a light microscope and representative images were taken. Adipocyte size in pgWAT was quantified using Adiposoft plugin on Fiji-Image J program (v. 2.1.0/1.53c), using criteria described by Parlee et al. [30].

2.5.2. Sirius red staining

Formalin-fixed liver tissues embedded in paraffin blocks and sectioned at 5 μm thickness were deparaffinized in xylene, rinsed with deionized water, and stained in solutions of phosphomolybdic acid for 2 min, picrosirius red F3BA stain for 60 min, and 0.1 N hydrochloride acid for 2 min. The stained slide was rinsed in 75% ethanol, dehydrated, air dried, and mounted with Depax mounting medium. Images were acquired with a light microscope.

2.5.3. Trichome staining

This was performed on formalin-fixed 5-μm liver sections. The sections were deparaffinized, rehydrated, and fixed for 1 h in Bouin's solution at 56 °C. The slides were stained with Weigert's iron hematoxylin, Biebrich scarlet-acid fuchsin, phosphomolybdic-phosphotungstic acid, and aniline blue solutions. The slides were washed in distilled water, dehydrated, and mounted with resinous mounting medium before images were acquired with a light microscope.

2.6. Liver and fecal lipid extraction and quantification

Lipid extraction from liver and feces were performed as described (11). Liver and fecal lipids were measured using colorimetric assays for triglycerides (Infinity; Thermo Scientific) and cholesterol (Cholesterol E; Wako), according to the manufacturer's instruction, and values were normalized by liver and fecal weight, respectively.

2.7. Fecal bomb calorimetry

Feces were collected from mice caged individually within a 24-h period during *ad libitum* feeding. Samples were dried for 48 h at 60^{0}C. Duplicate or triplicate samples of 45—55 mg were analyzed in Parr Instruments' 6725 Semimicro Calorimeter using a 1109 A Semimicro Oxygen Bomb placed in 450 g of water. The heat of combustion was generated in kCal/g.

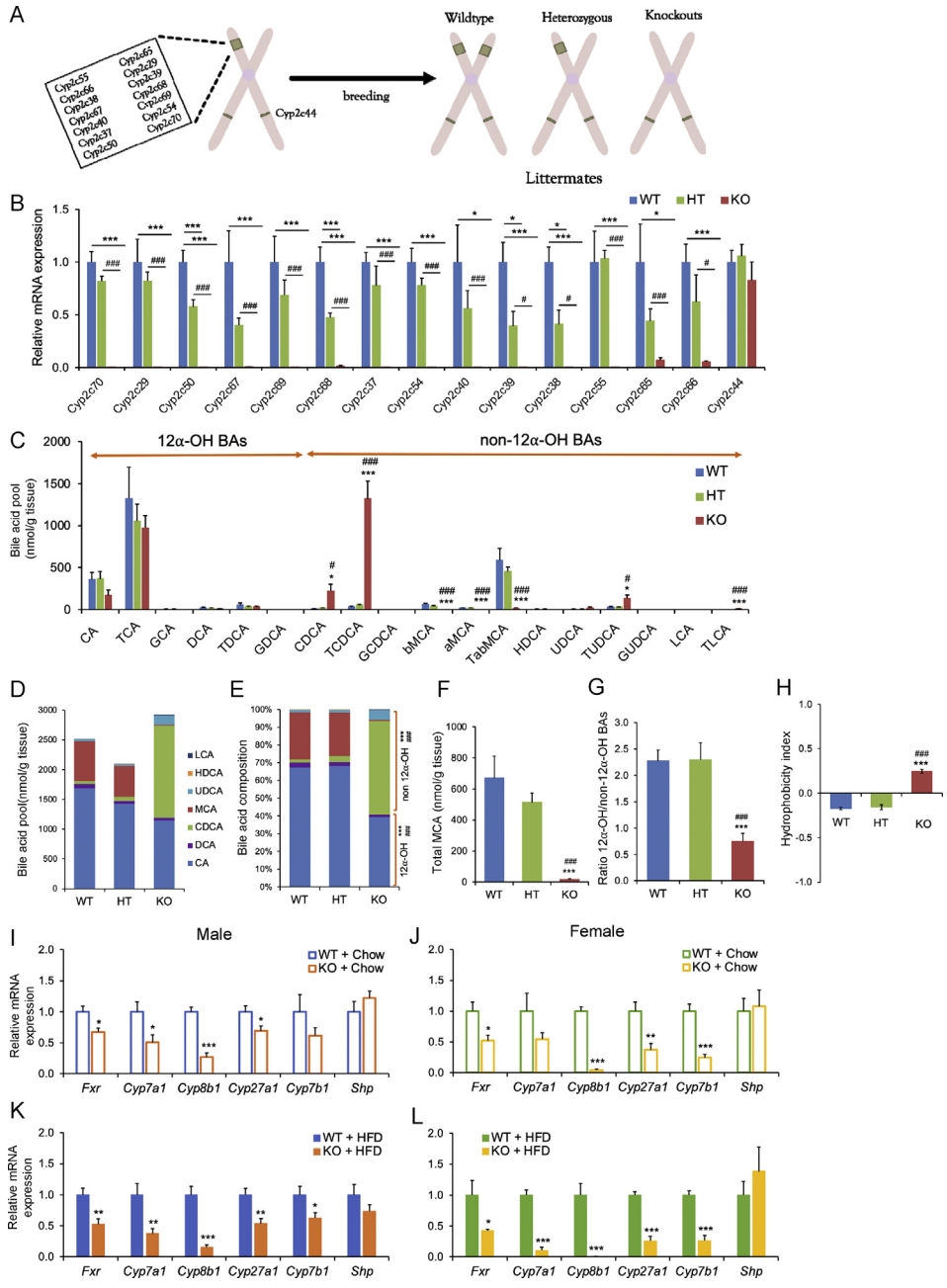

Figure 1: Cyp2c deficiency humanizes murine BA pool due to MCA depletion. A: Schematic of the 14 Cyp2c genes that were deleted in Cyp2c$^{-/-}$ model and the progeny genotypes from breeding heterozygotes. B: mRNA expression of Cyp2c genes in WT, Cyp2c$^{+/-}$, and Cyp2c$^{-/-}$ mice. C: BA species measured by UPLC-MS/MS from a pool of liver, gallbladder, and intestine. D—E: The absolute quantities (D) and relative proportions (E) of BAs. For D-F, each BA represents a total of unconjugated, taurine-conjugated, and glycine-conjugated subspecies. F: Total levels of all MCAs in WT, Cyp2c$^{+/-}$, and Cyp2c$^{-/-}$ mice. G: Ratio of total 12α-OH to total non-12α-OH BAs. H: Hydrophobicity index of BAs. I—L: Hepatic mRNA expression of BA metabolism genes in males on chow diet (I), females on chow diet (J), males on HFD (K), and females on HFD (L). Data are represented as mean $\pm$ SEM. n = 6 mice/group for B-H, 5-7 mice/group for I-L. *p $<$ 0.05, **p $<$ 0.01, and ***p $<$ 0.001 relative to WT and #p $<$ 0.05, and ###p $<$ 0.001 relative to Cyp2c$^{+/-}$. B—H by one-way ANOVA; I-L by Student's t-test.

2.8. RNA isolation and quantitative real-time PCR

Total RNA was isolated from mouse tissues using TRIzol reagent (Life Technologies). 2000 ng of RNA was used to synthesize cDNA by reverse transcription using high-capacity cDNA reverse transcription kit (Applied Biosystems). Gene expression was performed by quantitative PCR with iTaq Universal SYBR Green Supermix (Bio-Rad). Gene expression was normalized to *36b4* as a housekeeping gene. Primer sequences for measured genes are listed in Supplemental Table 1.

2.9. Statistical analysis

Data are presented as mean $\pm$ SEM. Statistical analysis by Student's t-test, one-way ANOVA, or two-way ANOVA followed by a Tukey's post hoc multiple comparison test. $p < 0.05$ is considered statistically significant.

Table 1 — Pooled bile acid profile by UPLC-MS/MS.

	WT	Cyp2c$^{+/-}$	Cyp2c$^{-/-}$
α-MCA	18.9 ± 3.9	19.1 ± 3.9	0.79 ± 0.01[b,d]
β-MCA	62.05 ± 11.7	38.2 ± 8.2	0.35 ± 0.01[b,d]
TαβMCA	589.0 ± 139.5	456.0 ± 53.2	16.1 ± 3.2[b,d]
CDCA	9.4 ± 1.4	17.0 ± 3.8	222.1 ± 77.9[a,c]
TCDCA	32.9 ± 8.8	55.1 ± 11.2	1322.3 ± 208.4[b,d]
GCDCA	n.d	0.27 ± 0.01	2.44 ± 0.7
CA (12α −OH)	360.4 ± 85.6	367.0 ± 89.2	170.0 ± 60.9
TCA (12α −OH)	1325.7 ± 368.4	1055.7 ± 200.1	976.0 ± 143.9
GCA (12α −OH)	3.9 ± 1.2	5.6 ± 2.7	3.1 ± 0.3
DCA (12α −OH)	20.2 ± 5.0	15.7 ± 4.4	7.4 ± 4.6
TDCA (12α −OH)	53.9 ± 23.5	32.7 ± 8.5	34.3 ± 11.0
GDCA (12α −OH)	0.25 ± 0.08	0.2 ± 0.04	0.2 ± 0.01
LCA	n.d	n.d	n.d
TLCA	0.3 ± 0.08	0.4 ± 0.1	11.0 ± 2.1[b,d]
UDCA	4.6 ± 0.9	6.1 ± 0.6	30.0 ± 15.2
TUDCA	31.0 ± 9.0	27.5 ± 3.8	137.3 ± 37.33[a,c]
GUDCA	n.d	n.d	n.d
HDCA	4.1 ± 0.2	4.5 ± 0.5	n.d
Total BAs	2513.6 ± 566.5	2096.1 ± 315.8	2922.2 ± 214.8
Conjugated BAs	2035.4 ± 532.6	1630.1 ± 253.9	2502.1 ± 236.3
Non conjugated BAs	478.2 ± 105.1	466.0 ± 105.5	420.1 ± 153.1
Primary BAs	2401.0 ± 545.1	2010.9 ± 302.2	2712.2 ± 193.8
Secondary BAs	112.6 ± 27.6	85.1 ± 15.6	210.0 ± 53.5
Total 12α-OH BAs	1762.9 ± 412.9	1474.0 ± 259.5	1190.2 ± 141.2
Total non-12α-OH BAs	750.7 ± 159.0	622.1 ± 73.0	1732.0 ± 211.7[b,d]

Values are means ± SE in nmol/g tissue. α-MCA, α-muricholic acid; β-MCA, β-muricholic acid; TαβMCA, tauro-α- and tauro-β-muricholic acid; CDCA, chenodeoxycholic acid; TCDCA, taurochenodeoxycholic acid; GCDCA, glycochenodeoxycholic acid; CA, cholic acid; TCA, taurocholic acid; GCA, glycocholic acid; DCA, deoxycholic acid; TDCA, taurodeoxycholic acid; GDCA, glycodeoxycholic acid; LCA, lithocholic acid; TLCA, taurolithocholic acid; UDCA, ursodeoxycholic acid; TUDCA, tauroursodeoxycholic acid; GUDCA, glycoursodeoxycholic acid; HDCA, hyodeoxycholic acid; BA, bile acid; n.d, not detected. Species marked "(12α-OH)" are 12α-hydroxylated, unmarked are non-12α-hydroxylated. [a]$p < 0.05$, [b]$p < 0.001$ vs. WT control; [c]$p < 0.05$, [d]$p < 0.001$ vs. Cyp2c$^{+/-}$ measured by one-way ANOVA.

3. RESULTS

3.1. Knockout of Cyp2c genes results in a human-like BA profile and a reduction in 12α-hydroxylated BAs

Heterozygous Cyp2c$^{+/-}$ mice were bred to generate Cyp2c$^{-/-}$, Cyp2c$^{+/-}$, and WT control mice (Figure 1A). Cyp2c44 is a member of this family of Cyp2c genes but is physically located outside the cluster and was therefore intact (Figure 1A). In the WT liver tissues, *Cyp2c29, Cyp2c37, Cyp2c38, Cyp2c40, Cyp2c50, Cyp2c54, Cyp2c69,* and *Cyp2c70* were highly expressed with cycle threshold (Ct) values of 22 or lower by qPCR. *Cyp2c67*, *Cyp2c39, Cyp2c55,* and *Cyp2c68* were moderately expressed, whereas *Cyp2c65* and *Cyp2c66* were lowly expressed with Ct values ∼35 in the WT mice. All of these mRNAs were modestly reduced in the Cyp2c$^{+/-}$ mice and undetectable in the Cyp2c$^{-/-}$ mice (Figure 1B). As expected, mRNA expression of *Cyp2c44*—which is located outside of the deleted gene cluster—did not differ between the 3 genotypes (Figure 1B).

UPLC-MS/MS analysis of BAs was performed on a pool of liver, gallbladder, and small intestine in males and females from each of the 3 genotypes. As shown in Supplemental Figure 1A and Supplemental Table 2, interindividual variability was high (as is known for BAs), but there were no sex-dependent differences in BA composition, so the male and female data were pooled together. The reduced expression of a number of Cyp2c genes in the Cyp2c$^{+/-}$ mice did not result in any significant changes in BA levels or composition compared to the WT mice, whereas the Cyp2c$^{-/-}$ mice showed significant changes in the BA composition compared to Cyp2c$^{+/-}$ and WT mice (Table 1 and Figure 1C,D). The levels of conjugated and unconjugated MCA were hardly detectable in the Cyp2c$^{-/-}$ mice, validating that the deletion of the Cyp2c cluster generates an MCA-deficient human-like BA profile (Figure 1C—F). On the other hand, there was an increase in the levels of conjugated and unconjugated CDCA in the Cyp2c$^{-/-}$ mice, consistent with CDCA being the predominant precursor for MCA synthesis (Figure 1C,D, E). Tauroursodeoxycholic acid (TUDCA) and taurolithocholic acid (TLCA)—which can be derived from CDCA—were increased in the Cyp2c$^{-/-}$ mice (Figure 1C,D, E). The absence of MCAs and a compensatory increase in CDCA demonstrate that Cyp2c$^{-/-}$ mice have a human-like BA pool.

We further characterized the BA pool composition based on other important physicochemical BA features. There were no differences between genotypes in the total amounts of conjugated or unconjugated BAs, and no differences in the total amounts of primary or secondary BAs (Table 1). In the Cyp2c$^{-/-}$ mice, a smaller portion of the BA pool was made up of BAs that are hydroxylated at the 12α-carbon position (12α-OH BAs)—cholic acid (CA), its secondary BA derivative DCA, and their conjugated forms (Figure 1E). These BAs are generated by the enzymatic activity of Cyp8b1, the 12α-hydroxylase. On the other hand, non-12α-OH BAs were significantly increased, leading to a significant decrease in the ratio of 12α-OH/non-12α-OH BAs (Figure 1G), consistent with what was observed in Cyp2c70-deficient mice [20,31]. MCA is considered a hydrophilic BA, therefore, its depletion and resultant alteration in BA composition increased the hydrophobicity index of BA pool in the Cyp2c$^{-/-}$ mice as calculated according to Heuman [32] (Figure 1H). Because there were no differences in BA profile between WT and Cyp2c$^{+/-}$ mice, subsequent experiments were conducted only in WT and Cyp2c$^{-/-}$ mice. Moreover, we conclude that partial reductions in the expression of Cyp2c genes are insufficient to modulate BA pool composition.

We also measured plasma BA composition. In both males and females, Cyp2c-deficiency resulted in barely detectable plasma MCA levels consistent with our findings from the total BA pool. On the other hand, there were increases in most other BA subspecies in Cyp2c$^{-/-}$ mice compared to controls, leading to a significant increase in total plasma BA levels (Supplemental Table 3), similar to what was observed in Cyp2c70-deficient mice [19].

To test whether changes in expression of BA metabolism genes could explain the altered BA composition in Cyp2c$^{-/-}$ mice, we measured the expression of key BA metabolism genes. In males and females on chow or HFD, there was a reduction of key BA synthesis genes *Cyp7a1*, *Cyp8b1, Cyp27a1,* and *Cyp7b1*, along with decreased expression of *FXR* in the liver of the Cyp2c$^{-/-}$ mice (Figure 1I-L). There were no significant changes in hepatic expression of *SHP* (Figure 1I-L), and there were no differences in ileal expression of *FXR* or *FGF15* between WT and Cyp2c$^{-/-}$ mice (data not shown). The reduction in *Cyp8b1* expression is consistent with the smaller proportion of 12α-OH BAs in Cyp2c$^{-/-}$ mice. We found decreases in several transcription factors that promote *Cyp8b1* expression, including *FoxO1*, *Nr5a2* (Lrh-1), *Hnf4a, Nr1i3* (CAR), and *Ppara* (Supplemental Figure. 1B—E), implicating a potential role of one or more of these transcription factors in the downregulation of *Cyp8b1*. We note that although female Cyp2c$^{-/-}$ mice had an apparently stronger suppression of *Cyp8b1* than male Cyp2c$^{-/-}$ mice did (versus female and male WT controls, respectively), this did not result in larger reductions in 12α-OH BAs (Supplemental Table 2), likely

because *Cyp8b1* expression and 12α-OH BA levels are not perfectly linearly correlated [16].

These changes in BA composition suggest that Cyp2c$^{-/-}$ mice may have alterations in intestinal lipid absorption that could affect susceptibility to HFD-induced obesity. The effects could be predicted to go in two opposing directions. Eliminating 12α-OH BAs from WT mice is known to reduce fat absorption [13,14,16]. Thus, the relative reduction in 12α-OH BAs in Cyp2c$^{-/-}$ mice suggests that they may be less susceptible to HFD-induced obesity. On the other hand, the increase in hydrophobicity of the BA pool when MCAs are absent might be predicted to enhance intestinal lipid absorption and promote obesity. We next investigated how the changes in BA composition affect obesity susceptibility and energy metabolism in the Cyp2c$^{-/-}$ mice.

3.2. Male Cyp2c$^{-/-}$ mice are resistant to HFD-induced obesity

In mice on chow diet, weekly body weight measurements showed no significant differences between WT and Cyp2c$^{-/-}$ mice in males (Figure 2A) or females (Figure 2B), and there were no differences in average food intake between the WT and Cyp2c$^{-/-}$ mice in either sex (Figure 2C,D). Body composition analysis showed no differences in lean and fat mass between the genotypes in chow-fed males, but chow-fed female Cyp2c$^{-/-}$ mice had slightly higher lean mass than WT controls (Figure 2E,F).

In a parallel study conducted in the second cohort of mice fed a HFD (60% of kcal derived from fat) for 18 weeks, body weights of males diverged after just one week, such that male WT mice gained substantial body weight, whereas male Cyp2c$^{-/-}$ mice were protected (Figure 2G). Female mice of both genotypes were protected from obesity (Figure 2H). We did not detect any significant difference in average food intake between genotypes (Figure 2I,J). Prior to HFD intervention, fat mass was similar between genotypes, but after 17 weeks on HFD, fat mass was significantly lower in Cyp2c$^{-/-}$ males compared to WT controls (Figure 2K). We did not observe any significant differences between genotypes in females (Figure 2L). Lean mass did not differ between the genotypes (Figure 2M, N). This demonstrates that the low body weight of male Cyp2c$^{-/-}$ mice was due to low adiposity.

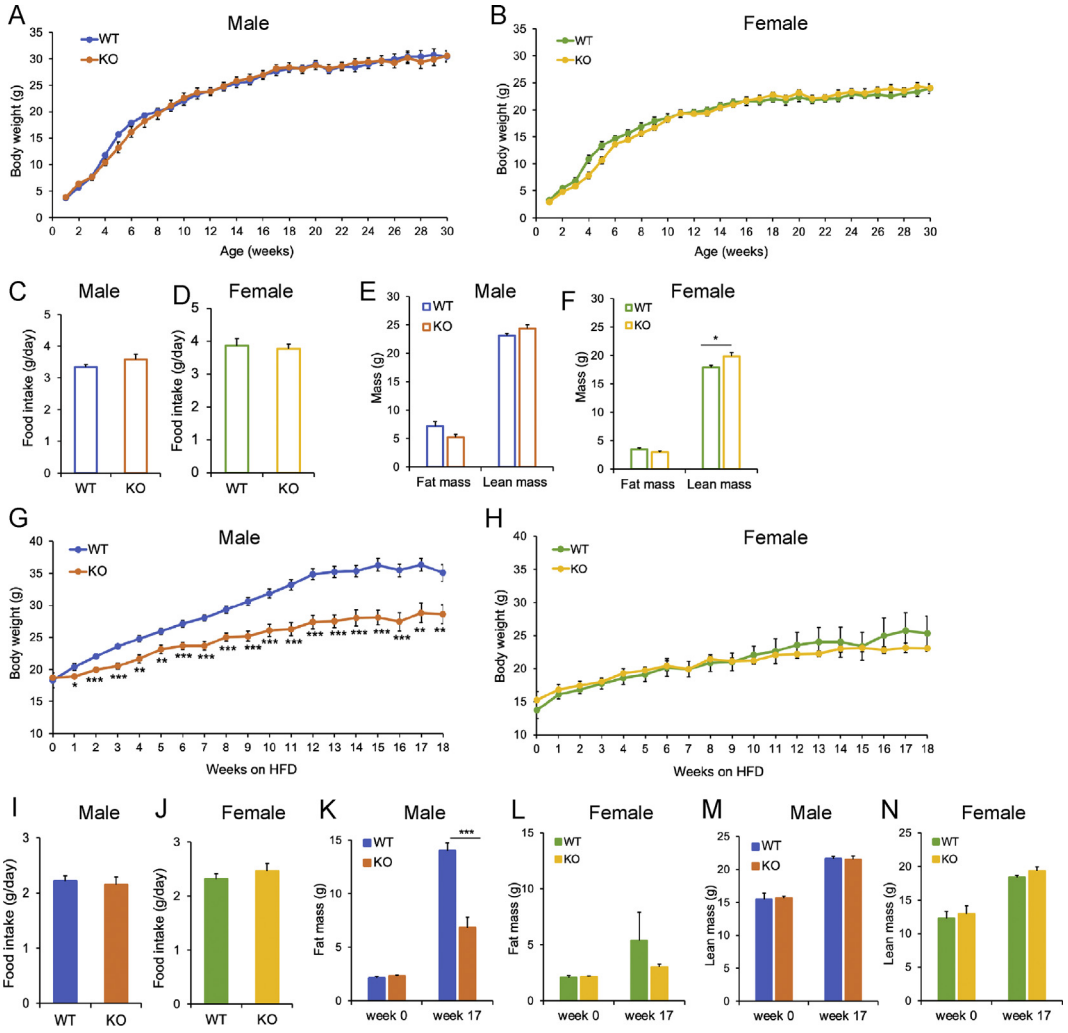

Figure 2: Cyp2c deficiency protects against diet-induced obesity in male mice. A—B: Weekly body weight in male (A) and female (B) mice on chow diet. C—D: Average daily food intake in male (C) and female (D) chow-fed mice. E—F: Fat and lean mass in male (E) and female (F) chow-fed mice. G—H: Weekly body weight in male (G) and female (H) fed HFD. I—J: Average daily food intake in male (I) and female (J) mice fed HFD. K—L: Fat mass in males (K) and females (L) before and after 17 weeks on HFD. M—N: Lean mass in males (M) and females (N) before and after 17 weeks on HFD. Data are represented as mean ± SEM. n = 7 mice/group for all groups, except n = 5 mice/group for females + HFD. *p < 0.05, **p < 0.01, and ***p < 0.001 relative to WT by Student's t-test.

3.3. Male and female Cyp2c$^{-/-}$ mice show improvements in glucose homeostasis

Cyp2c$^{-/-}$ male mice showed significant improvements in OGTT on both chow and HFD (Figure 3A,B) as well as improvements in ITT on chow diet but not on HFD (Figure 3C,D). Cyp2c$^{-/-}$ females on both chow and HFD showed lower glucose 15 min after glucose gavage during OGTT, but no significant difference in total area under the curve (Figure 3E,F). Cyp2c$^{-/-}$ females also showed improved ITT on chow diet but not on HFD (Figure 3G,H). To investigate a potential change in first-phase insulin response during OGTT, we measured plasma insulin before and after a 15-minute oral glucose challenge in chow-fed mice. Whereas Cyp2c$^{-/-}$ mice showed significantly lower blood glucose 15 min after glucose delivery compared to WT controls, there were no significant differences between genotypes in plasma insulin (Figure 3I,J). This suggests that the improved glucose homeostasis is independent of enhanced pancreatic beta cell function.

To assess whether these improvements in OGTT were specific to an incretin effect, we also performed IPGTTs. Male Cyp2c$^{-/-}$ mice showed improved IPGTTs on both diets compared to WT (Supplemental Figure 2A and B), and males of all diets and genotypes showed a strong incretin effect (Supplemental Figure 2C–F). In females, there were no differences in IPGTT between genotypes (Supplemental

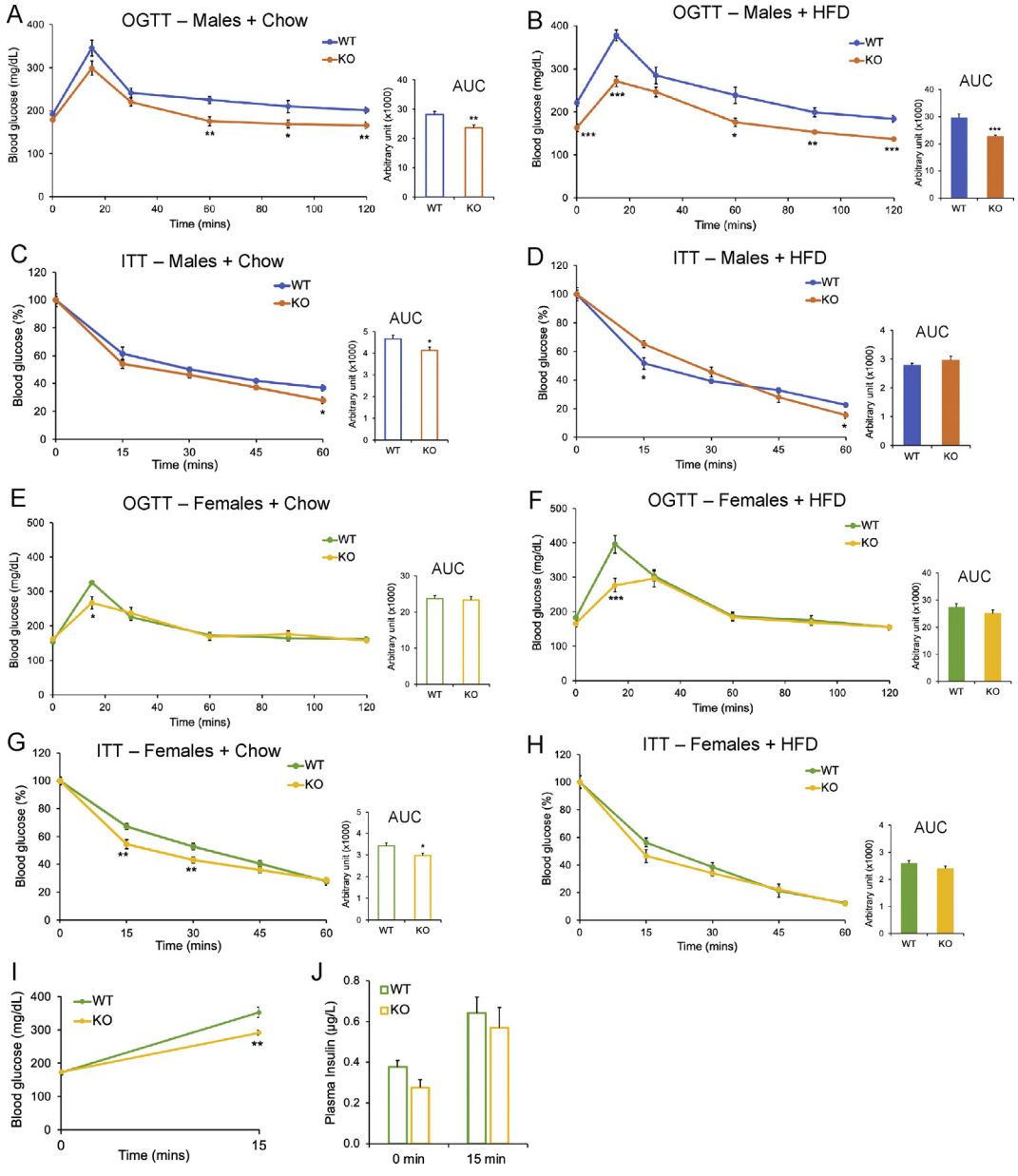

Figure 3: Cyp2c deficiency improves systemic glucose homeostasis independent of diet and sex. A: OGTT in 24-week-old male mice on chow diet. B: OGTT in male mice after 12 weeks on HFD. C: ITT in 26-week-old male mice on chow diet. D: ITT in male mice after 14 weeks on HFD. E: OGTT in 24-week-old female mice on chow diet. F: OGTT in female mice after 12 weeks on HFD. G: ITT in 26-week-old female mice on chow diet. H: ITT in female mice after 14 weeks on HFD. Insets represent the area under the curve (AUC). I–J: Blood glucose (I) and plasma insulin (J) measured before and 15 min after oral glucose challenge in 8-week-old chow-fed female mice. Data are represented as mean ± SEM. n = 7 mice/group for all groups, except n = 5 mice/group for females + HFD, and n = 6 mice/group for I and J. *p < 0.05, **p < 0.01, and ***p < 0.001 relative to WT by Student's t-test.

Figure 2G and H), and no incretin effect on either diet (Supplemental Figure 2I-L).

We further analyzed plasma samples obtained from mice that were fasted for 5 h. Under chow diet conditions, there were no differences in blood glucose or plasma insulin between genotypes, but under HFD conditions, Cyp2c$^{-/-}$ male but not Cyp2c$^{-/-}$ female mice showed significantly lower levels of blood glucose and plasma insulin compared to WT controls (Figure 4A,B).

The improvements in glucose tolerance that we observed in Cyp2c$^{-/-}$ mice were present in those at lower body weight than controls (*e.g.,* Cyp2c$^{-/-}$ males fed HFD) and in those at the same body weight as controls (*e.g.,* Cyp2c$^{-/-}$ males on chow and females on both diets). As a further test of the improvements in glucose tolerance—and whether they are independent of body weight—we examined mice on a western diet, which is lower in fat than the HFD. There were no significant differences in body weight between genotypes (Supplemental Figure 3A and B). However, Cyp2c$^{-/-}$ males and females still showed improvements in OGTT and IPGTT compared to WT controls (Supplemental Figure 3C—F). There were no differences in ITT or 5-hour fasted blood glucose and plasma insulin levels between genotypes (Supplemental Figure 3G—J). Taken together, these data suggest that Cyp2c$^{-/-}$ mice of both sexes have improvements in systemic glucose tolerance that are independent of incretin hormones and independent of body weight.

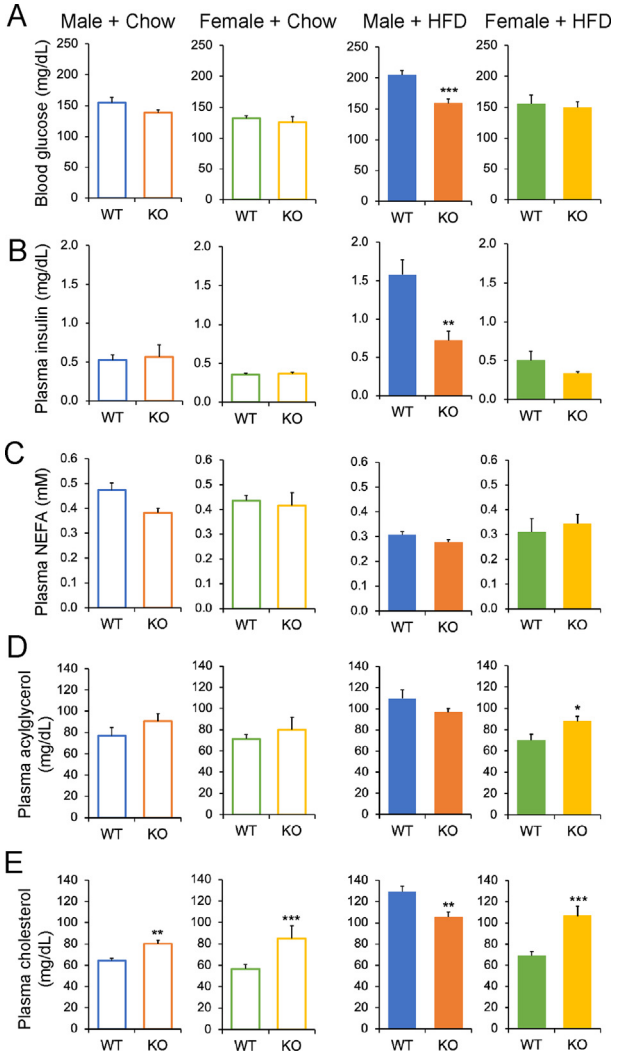

Figure 4: Effects of Cyp2c deficiency on plasma metabolites and insulin. A—E: Blood glucose (A) and plasma levels of insulin (B), NEFA (C), acylglycerol (D), and cholesterol (E) in males and females fed chow or HFD, after a 5-hour fast. Data are represented as mean ± SEM. n = 7 mice/group for all groups, except n = 5 mice/group for females + HFD. *p < 0.05, **p < 0.01, and ***p < 0.001 relative to WT by Student's t-test.

3.4. Cyp2c-deficiency alters plasma lipoprotein profile

After a 5-hour fast, plasma levels of NEFA did not differ between the mice (Figures 4C). On chow diet, plasma acylglycerols did not differ between genotypes, but on HFD, plasma acylglycerols were significantly increased in the Cyp2c$^{-/-}$ females compared to WT controls (Figure 4D). Plasma cholesterol was increased in Cyp2c$^{-/-}$ males on chow diet and Cyp2c$^{-/-}$ females on chow and HFD, showing that the lack of MCAs generally raises circulating cholesterol [20,21]. On the other hand, under HFD conditions, WT males had high cholesterol levels, and this was significantly blunted in the Cyp2c$^{-/-}$ males, possibly as a secondary consequence to their obesity resistance. In the western diet cohort, Cyp2c$^{-/-}$ females showed significant increases in plasma levels of acylglycerol, cholesterol, and NEFA compared to WT controls (Supplemental Figure 3K-M).

We next examined lipoprotein subfractions. In general, we found that Cyp2c$^{-/-}$ mice had higher levels of cholesterol and acylglycerol in LDL fractions, and this effect was stronger in females (Figure 5A—H). To test for potential explanations for the changes in the lipoprotein profile, we measured mRNA expression of key cholesterol metabolism genes. While the transcription factor Srebp2 and several of its target genes were not different between genotypes, we found that LDL receptor (*LDLR*) expression tended to be decreased in Cyp2c$^{-/-}$ mice (Figure 5I-L). These data suggest that the lack of MCAs may lower the clearance of LDL particles via reductions in hepatic *LDLR*, as previously suggested [20,21].

3.5. Resistance of Cyp2c$^{-/-}$ male mice to HFD-induced obesity protects against adipose inflammation

Cyp2c$^{-/-}$ mice tended to have reductions in relative gonadal fat mass in both sexes (Figure 6A). Chronic low-grade inflammation and infiltration of immune cells are well-known hallmarks of increased adiposity [34,35]. Consistent with this, we observed crown-like structures (Figure 6B) and increased adipocyte size in the gonadal fat of the HFD-fed male WT mice but not in other male groups or female groups (Figure 6C,D). In line with the histology, the obesity-sensitive male WT mice showed a strong increase in expression of inflammatory genes such as *F4/80*, *Cd68*, *Mcp1,* and tumor necrosis factor alpha (*Tnfa*), but not in the other male groups or female groups (Figure 6E,F). It has been reported that in obesity, de novo lipogenesis in the fat tissue is repressed [36,37]. In agreement, lipogenic genes such as *Srebp1c* and its downstream targets trended toward decreased expression in the HFD-fed male WT mice, but this effect was blunted in the non-obese male and female groups (Figure 6G,H). Taken together, Cyp2c$^{-/-}$ male mice show adipose tissue phenotypes consistent with their decreased obesity.

3.6. Energy balance

To examine the mechanisms of reduced HFD-induced obesity in the male Cyp2c$^{-/-}$ mice, we performed indirect calorimetry in male mice. We detected no significant differences in energy expenditure between the genotypes on chow diet (Figure 7A) or HFD (Figure 7B), and as shown in Supplemental Figure 4A—F. Additionally, the histological staining of BAT (Supplemental Figure 4G) and the expression of

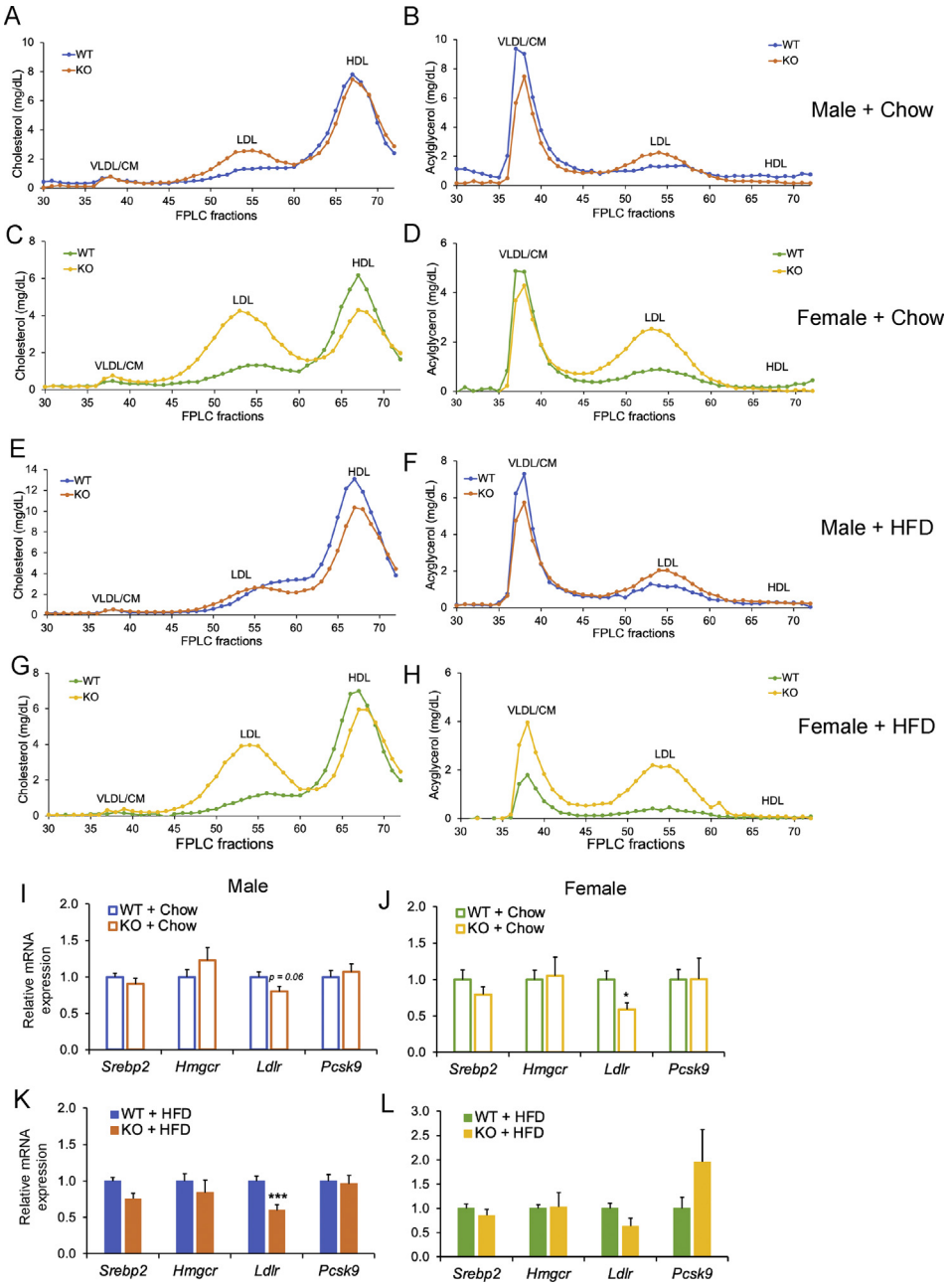

Figure 5: Cyp2c-deficiency alters lipoprotein profile. A—B: Plasma cholesterol (A) and acylglycerol (B) in FPLC fractions of male chow-fed mice. C—D: Plasma cholesterol (C) and acylglycerol (D) in FPLC fractions of female chow-fed mice. E—F: Plasma cholesterol (E) and acylglycerol (F) in FPLC fractions of male HFD-fed mice. G—H: Plasma cholesterol (G) and acylglycerol (H) in FPLC fractions of female HFD-fed mice. I—L: Hepatic mRNA expression of cholesterol metabolism genes in males on chow diet (I), females on chow diet (J), males on HFD (K), and females on HFD (L). Data are represented as mean ± SEM. n = 7 mice/group for all groups, except n = 5 mice/group for females + HFD. *$p < 0.05$, **$p < 0.01$, and ***$p < 0.001$ relative to WT by Student's t-test.

thermogenic genes showed no differences between the groups on either chow or HFD (Supplemental Figure 4H and I).

Because we observed substantial protection from HFD-induced obesity in Cyp2c$^{-/-}$ males, but no significant differences in food intake or energy expenditure, we reasoned that there may be an increase in calorie excretion. However, bomb calorimetry showed no significant differences in fecal energy output between the Cyp2c$^{-/-}$ mice and WT controls on either chow or HFD (Figure 7C). There were no differences in average total fecal production between genotypes (Supplemental Figure 4J). Our interpretation of these unexpected findings is that male Cyp2c$^{-/-}$ mice on a HFD have slight changes in food intake, energy expenditure, calorie excretion, or all three, that are below the limit of detection in these assays, but that add up over time to significant protection from obesity.

3.7. Cyp2c$^{-/-}$ mice have impaired intestinal lipid absorption, which can be rescued by taurocholic acid

A key premise of this study is that MCAs are thought to promote poor lipid absorption, and therefore eliminating MCAs and shifting the mouse BA pool to other types of BAs may be predicted to enhance lipid

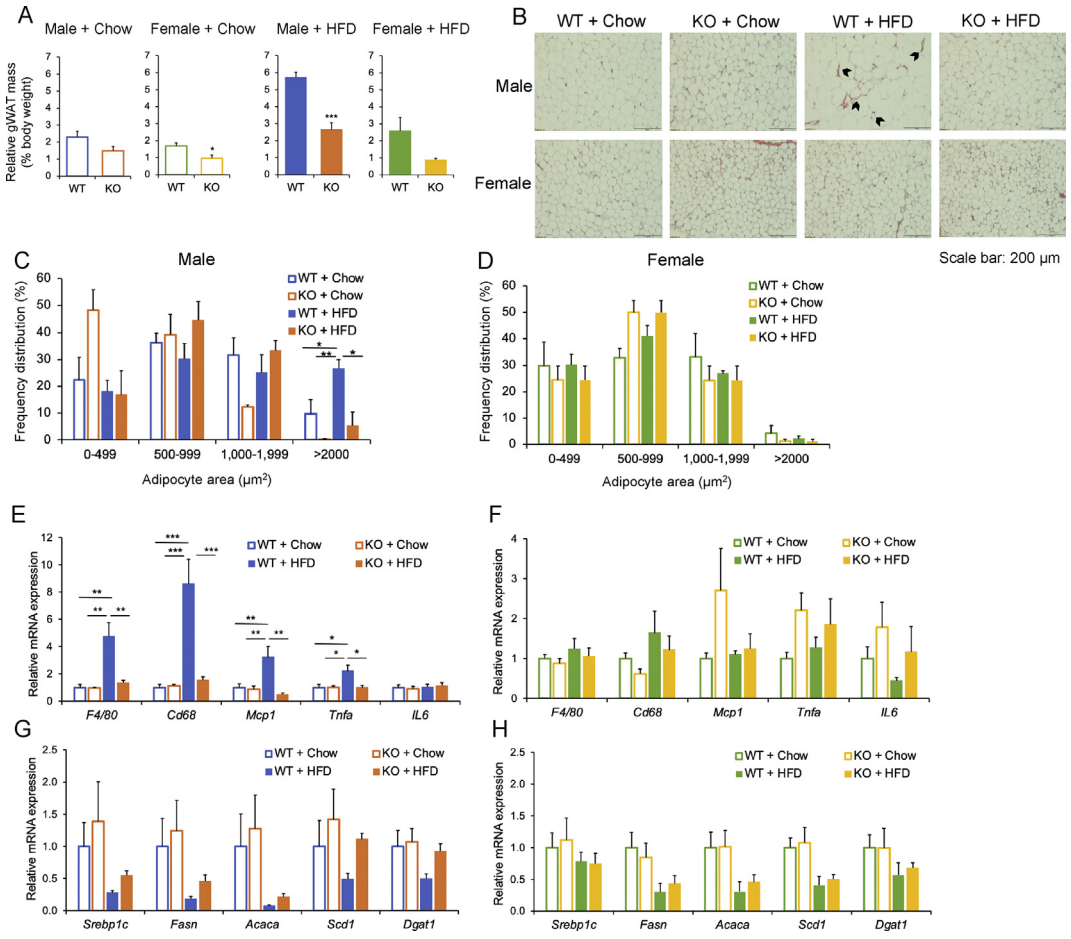

Figure 6: Resistance to obesity in Cyp2c$^{-/-}$ mice protects against adipose tissue inflammation. A: Gonadal white adipose tissue (gWAT) mass relative to body weight in males and females fed chow or HFD. B: Representative images of H & E staining of gWAT in males and females. Scale bar is 200 μm. C—D: Adipocyte size distribution in perigonadal adipocytes in male (C) and female (D) mice. E—F: mRNA expression of pro-inflammatory genes in gWAT of males (E) and females (F) on chow or HFD. G—H: mRNA expression of lipogenesis genes in gWAT of male (G) and female (H) on chow diet or HFD. Data are represented as mean ± SEM. n = 7 mice/group for all groups, except n = 5 mice/group for females + HFD. *p < 0.05, **p < 0.01, and ***p < 0.001 by two-way ANOVA and Tukey's multiple comparisons test.

absorption. To pursue this, we quantified fecal lipids. During chow feeding, there were no changes in fecal acylglycerol, cholesterol, or NEFA between the two genotypes (Figure 7D—F). However, in Cyp2c$^{-/-}$ males and females on western diet, and in Cyp2c$^{-/-}$ males on HFD, fecal acylglycerol, and cholesterol content, but not NEFA, were significantly increased in the stool (Figure 7D—F, Supplemental Figure 3N—P), suggesting that under HFD conditions, Cyp2c$^{-/-}$ may have increased lipid excretion and reduced lipid absorption compared to WT controls.

To further assess whether Cyp2c$^{-/-}$ mice have reduced intestinal lipid absorption, we performed two additional experiments. First, we performed a fasting re-feeding experiment. Following an overnight fast (~14 h), plasma levels of acylglycerol (Figure 7G) and NEFA (Figure 7H) did not differ between WT and Cyp2c$^{-/-}$ mice. After 2 h of re-feeding HFD, plasma acylglycerol, and NEFA were significantly lower in the Cyp2c$^{-/-}$ mice (Figure 7G,H), consistent with reduced intestinal lipid uptake.

In the second experiment, we used a radiolabeled triolein to directly measure intestinal lipid absorption. We fasted mice for 4 h, injected them with poloxamer 407 to block lipoprotein clearance, then administered olive oil containing a radiolabeled triglyceride, [^{3}H] triolein, by oral gavage. The Cyp2c$^{-/-}$ mice showed significantly lower plasma levels of [^{3}H] at 8- and 24-hours post-gavage, demonstrating reduced absorption of intestinal triglyceride compared to WT (Figure 7I).

We reasoned that the impaired triglyceride absorption in the Cyp2c$^{-/-}$ mice could be due to their reduction in the ratio of 12α-OH/non-12α-OH BAs. To test whether increasing 12α-OH BAs in Cyp2c$^{-/-}$ mice rescues their defect in intestinal lipid absorption, WT and Cyp2c$^{-/-}$ mice received an oral gavage of either a low dose (17 mg/kg) of TCA or vehicle for 3 consecutive days. The 17 mg/kg dose was used because of previous reports that this dose elevates levels of CAs without changing the total BA levels [26,27]. We validated the dosing protocol by measuring the total BA pool composition. We found that TCA gavage in this dosing protocol caused no differences in total BA pool size, but successfully raised the levels of 12α-OH BAs and tripled the ratio of 12α-OH/non-12α-OH BAs in the Cyp2c$^{-/-}$ mice (Figure 7J-L and Supplemental Table 4). The TCA-gavage treatment did not alter the hydrophobicity index of the WT mice, but made the Cyp2c$^{-/-}$ BA pool slightly more hydrophilic (Figure 7M). Having validated the dosing strategy, we performed lipid absorption tests. Compared to Cyp2c$^{-/-}$ mice gavaged with vehicle control, the TCA gavage rescued the lipid absorption of Cyp2c$^{-/-}$ mice, as demonstrated by the lack of any differences in radioactive tracers in the plasma of the Cyp2c$^{-/-}$ mice

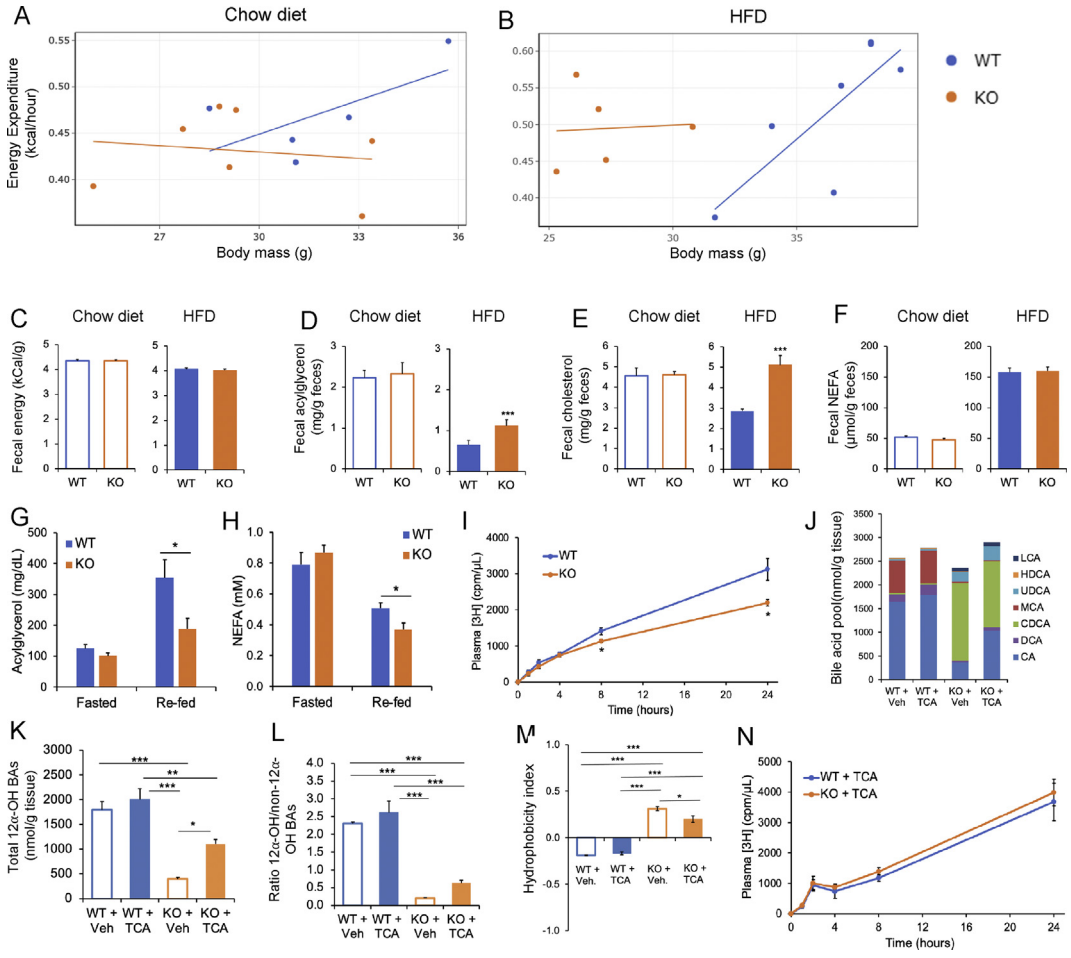

Figure 7: Indirect calorimetry and lipid absorption analyses in male Cyp2c$^{-/-}$ mice. A—B: Average hourly energy expenditure via indirect calorimetry over a 4-day period in 29-week-old mice on chow diet (A) and mice after 17 weeks on HFD. (B). C: Fecal energy content by bomb calorimetry in 29-week-old mice on chow diet and in mice after 17 weeks on HFD. D—F: Fecal levels of acylglycerol (D), cholesterol (E), and NEFA (F) in 29-week-old chow-fed mice and in mice after 17 weeks on HFD. G—H: Plasma levels of acylglycerol (G) and NEFA (H) in 12-week-old mice fasted overnight for 14 h and re-fed HFD for 2 h. I: Plasma levels of [^{3}H] in 10-week-old mice undergoing the radiolabeled triolein absorption experiment. J—M: BA levels from a pool of liver, gallbladder, and intestine (J), total 12α-OH BAs (K), ratio of total 12α-OH to total non-12α-OH BAs (L), and hydrophobicity index (M) in mice orally gavaged with low dose (17 mg/kg) TCA or vehicle control (Veh) for 3 consecutive days. N: Plasma levels of [^{3}H] in mice orally gavaged with TCA or vehicle control (Veh) followed by radiolabeled triolein absorption experiment. Data are represented as mean ± SEM. n = 5–7 mice/group for A-F, 5-6 mice/group for G—I & N, and 4 mice/group for J—M. *p < 0.05, **p < 0.01, and ***p < 0.001 relative to WT by Student's t-test for A—I & N, and by two-way ANOVA for J—M.

compared to WT (Figure 7N). This indicates that increasing the levels of 12α-OH BAs is sufficient to rescue the impaired lipid absorption in Cyp2c$^{-/-}$ mice. Taken together, Cyp2c deficiency and the resultant relative reduction in 12α-OH BAs promote fecal lipid excretion and reduce intestinal lipid absorption.

3.8. Cyp2c$^{-/-}$ mice have liver injury

The liver is central to lipid and BA metabolism and therefore responsive to modulated BA metabolism. Compared to WT controls, liver mass relative to body weight was increased in Cyp2c$^{-/-}$ mice (Figure 8A). This was not due to the accumulation of excess hepatic lipid, as acylglycerols were significantly reduced in Cyp2c$^{-/-}$ mice (Figure 8B). Liver cholesterol did not differ between genotypes in male mice, but female Cyp2c$^{-/-}$ mice showed a significant reduction in liver cholesterol under HFD condition (Figure 8C). Decreases in liver acylglycerol and cholesterol were also observed in Cyp2c$^{-/-}$ males and females that fed a western diet compared to littermate controls (Supplemental Figure 3Q, R).

Because Cyp2c$^{-/-}$ mice showed low liver fat, even in conditions when body weights were normal, it suggested possible liver-intrinsic alterations in fat handling, which we then investigated. Liver VLDL-triglyceride secretion showed no differences between Cyp2c$^{-/-}$ mice and WT controls (Supplemental Figure 5A). Cyp2c$^{-/-}$ mice tended to have decreased hepatic mRNA expression of enzymes involved in both de novo lipogenesis and fatty acid oxidation (Supplemental Figure 5B—E). This suggests that the low liver fat in Cyp2c$^{-/-}$ mice may involve reduced lipid synthesis, rather than increased lipid oxidation or secretion.

Increased hepatotoxicity has been reported in mice fed diets supplemented with LCA [38,39]. In rat hepatocytes, CDCA has induced hepatotoxicity more potently than other BAs [40]. Because CDCA and TLCA levels are elevated in Cyp2c$^{-/-}$ mice, we assessed liver

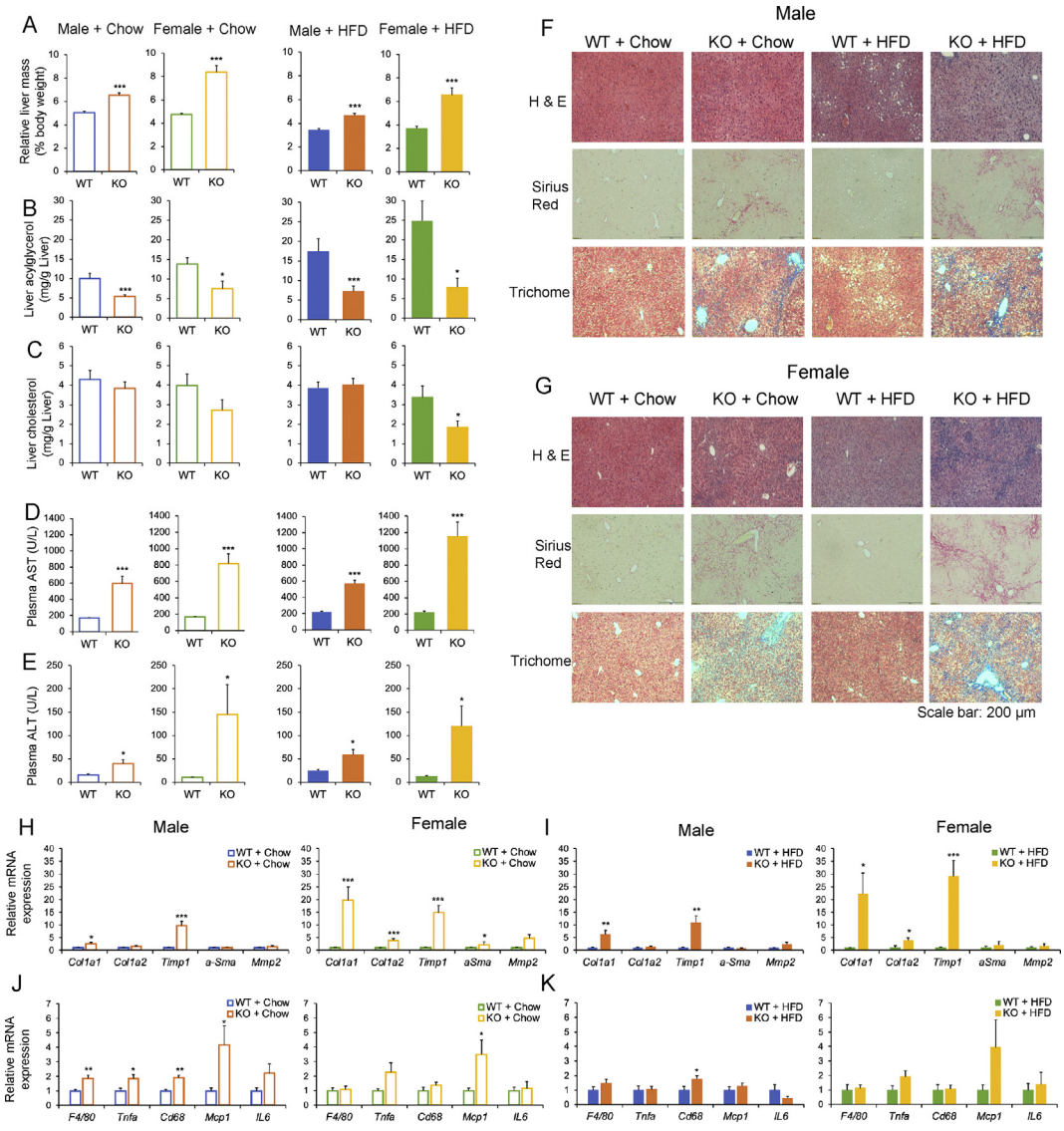

Figure 8: Cyp2c$^{-/-}$ mice have liver injury. A: Liver mass relative to body weight in males and females on chow or HFD. B: Hepatic acylglycerol in male and female mice on chow or HFD. C: Hepatic cholesterol in male and female mice on chow or HFD. D: Plasma AST levels in male and female mice on chow or HFD. E: Plasma ALT levels in male and female mice on chow or HFD. F—G: Representative images from H & E, Sirius red, and trichome stainings in males (F) and females (G) fed chow or HFD. Scale bar is 200 μm. H—I: Hepatic mRNA expression of fibrosis genes in male and female mice on chow (H) and male and female on HFD (I). J—K: Hepatic mRNA expression of pro-inflammatory genes in male and female mice on chow (J) and male and female on HFD (K). Data are represented as mean ± SEM. n = 7 mice/group for all groups, except n = 5 mice/group for females + HFD. *p < 0.05, **p < 0.01, and ***p < 0.001 relative to WT by Student's t-test.

damage. Plasma levels of liver enzymes AST and ALT were significantly increased in both male and female Cyp2c$^{-/-}$ mice in a diet-independent manner with the females showing stronger elevations compared to males (Figure 8D,E). In male mice, Cyp2c deficiency resulted in mild liver fibrosis, as evidenced by increased collagen deposition in Sirius red and trichome stains (Figure 8F). In female mice, Cyp2c deficiency caused strong liver fibrosis (Figure 8G). In agreement with the histological data, mRNA expression of fibrosis gene markers corroborated the mild fibrosis in the Cyp2c$^{-/-}$ male mice and the strong fibrosis in the Cyp2c$^{-/-}$ female mice (Figure 8H—I). Additionally, there were a modest increase in inflammatory gene markers in the Cyp2c$^{-/-}$ male and female mice (Figure 8J,K). Taken together, Cyp2c deficiency leads to increased hepatic injury, which is more severe in females than males.

4. DISCUSSION

In this study, we confirm the depletion of MCAs in Cyp2c-deficient mice, and further show that mice that are heterozygous for Cyp2c retain their ability to synthesize normal levels of MCAs, despite 50% decreases in the expression of most Cyp2c genes. Furthermore, we show that contrary to predictions, MCA *depletion* results in impaired lipid absorption and protection against HFD-induced obesity in male mice. Additionally, Cyp2c deficiency promotes mild and severe liver injury in male and female mice, respectively, consistent with a recent publication [31]. Regarding sex differences, we found that most effects of Cyp2c depletion occurred in both sexes, suggesting more similarities than differences. While the protection from HFD-induced obesity that we observed was in males, we cannot rule out that under

conditions where female WT mice become obese, and female Cyp2c$^{-/-}$ mice may be protected.

Published studies have suggested that mice with high levels of MCAs are protected against HFD-induced obesity [15,16], potentially because MCAs are considered hydrophilic BAs that are predicted to poorly promote intestinal lipid absorption. However, those studies indirectly raised MCAs, as a secondary consequence of Cyp8b1 deletion. Our study directly investigates the role of MCAs in the obesogenic diet response by using mice that lack MCAs. Our results disagree with the prediction that MCAs protect against obesity. We found that in both males and females, the absence of MCA did not promote obesity. In fact, in males, the absence of MCA *protected* against HFD-induced obesity and the associated chronic low-grade inflammation of the adipose tissue. We tested whether this protection was explained by increased energy expenditure, decreased food intake, or increased calorie excretion, but did not find a significant difference in any single parameter that could explain the low body weight. Moreover, our analysis of mice fed chow, where there were no differences in body weight between genotypes, did not reveal a clear genotype-specific energy balance parameter in Cyp2c$^{-/-}$ mice that would prevent weight gain upon HFD exposure. Our interpretation is that mild differences in some or all of these parameters likely exist but are not detectable with our instruments and statistical power. Of note, the absence of MCA disrupted the relationship between energy expenditure and body mass. In WT C57Bl/6 mice, larger mice require greater levels of energy expenditure [41]. However, this correlation is not observed in Cyp2c-deficient mice (Figure 7A and B). A similar effect was observed in mice engineered with a microbiome lacking a bile salt hydrolase [42], suggesting a possible role for the microbiome that will be of interest for future studies.

We also directly tested the expectation, based on prior publications, that lack of MCAs would raise the hydrophobicity of the BA pool and consequently increase intestinal lipid absorption. Our results showed the opposite effect—the lack of MCAs did increase in the BA hydrophobicity index, but this was associated with a decrease in intestinal triglyceride absorption. We conclude that the hydrophobicity index of a BA pool is insufficient to explain the functional effects of BAs on intestinal lipid absorption.

On the other hand, in Cyp2c$^{-/-}$ mice, there is a significant decrease in the ratio of 12α-OH/non-12α-OH BAs. This phenotype is likely due to the strong repression of Cyp8b1, the enzyme responsible for synthesizing 12α-OH BAs, as previously suggested [20,21]. Indeed, studies in mice from our group and others have shown that knockout of Cyp8b1 depletes the murine BA pool of 12α-OH BAs, and this leads to reduced intestinal lipid absorption, lower body weight, and improvements in cardiometabolic parameters [14–17]. Thus, the decreased lipid absorption of Cyp2c$^{-/-}$ mice is consistent with the reduced ratio of 12α-OH/non-12α-OH BAs in these mice. This is further supported by our finding that an oral gavage of TCA, the major 12α-OH BA, rescues the intestinal lipid absorption in the Cyp2c$^{-/-}$ mice. In future studies, it will be of interest to determine whether Cyp2c$^{-/-}$ mice exhibit alterations in the absorption of macronutrients other than lipids. Altogether, these data suggest that 12α-OH BA content of the BA pool is more important than the hydrophobicity index for regulating the efficiency of intestinal lipid absorption.

Our work shows that Cyp2c deficiency also causes other interesting metabolic effects. For one thing, it causes a more human-like LDL-cholesterol-enriched lipoprotein profile, particularly in females. In our study as well as the studies in Cyp2c70-deficient mice, observed downregulation of the LDLR potentially contributes to the elevated LDL cholesterol [21,31]. Another change we observed was the improvement in glucose metabolism. This improvement appears to be independent of body weight, as we observed in chow-fed and western diet-fed Cyp2c$^{-/-}$ mice, which have no differences in body weight compared to controls. This effect is also somewhat contrary to what might be predicted based on the literature. Prior studies have shown that glycine and taurine conjugated β-MCA can antagonize intestinal FXR leading to improvements in glucose homeostasis and metabolic disorders [11,43]. Our data suggest that MCA *depletion* confers improved glucose homeostasis. Future studies will be required to determine the mechanisms of this improvement, but it appears to be independent of the intestine, based on our OGTT and IPGTT data.

Finally, our study shows liver damage in the Cyp2c$^{-/-}$ mice, which appears more severe in females than males as also recently reported in Cyp2c70-deficient mice [31]. It has previously been observed that elevated levels of certain BAs including LCA and CDCA can be hepatotoxic [38,39]. Thus, the increases in CDCA and LCA may contribute to the liver damage phenotypes in the Cyp2c$^{-/-}$ mice as others have suggested in Cyp2c70-deficient mice [31]. Because Cyp2c enzymes are also involved in drug metabolism and detoxifying xenobiotics [44,45], we cannot rule out that these roles also contribute to the effects of Cyp2c deletion on liver damage.

We observed several similarities between the Cyp2c$^{-/-}$ mice and the published Cyp2c70-deficient mice. These include similar phenotypes such as depletion of MCAs, reduced BA 12α-hydroxylation, reduced expression of BA metabolism genes, increased LDL, and increased liver damage [20,21,31]. Based on those phenotypes, knockout of Cyp2c70 appears to mimic knockout of the Cyp2c gene cluster, although in the absence of parallel experiments, it is difficult to make final conclusions.

In conclusion, our study shows that the absence of MCA in Cyp2c-deficient mice results in altered BA composition characterized by decreased ratio of 12α-OH/non-12α-OH BAs. In male mice, this is associated with resistance to HFD-induced obesity and reduced intestinal lipid absorption. Therefore, data from this study (i) do not support the purported anti-obese effect of MCA and (ii) suggest that the 12α-OH BA content of the BA pool overrules hydrophobicity in the regulation of lipid absorption.

AUTHOR CONTRIBUTIONS

Antwi-Boasiako Oteng designed the study, performed experiments, analyzed the data, and drafted the manuscript. Sei Higuchi performed experiments. Alexander S. Banks supervised experiments and analyzed data. Rebecca A. Haeusler designed the study, provided supervision, and revised the manuscript. All authors have read, edited, and approve of the final manuscript.

ACKNOWLEDGMENTS/GRANT SUPPORT

This work was supported by NIH grants R01 DK115825 to RAH, T32 DK07559 to A-BO, S10OD028635 to ASB, and facilities/instrumentation supported by UL1TR001873, P30DK063608, P30DK026687, and American Diabetes Association grant 7-20-IBS-130 to RAH. We are grateful to Columbia University Biomarkers Core Laboratory and the Core Lab director Renu Nandakumar for assistance with the BA profiling and Utpal Pajvani and other members of the Haeusler Lab for discussions of the data.

CONFLICT OF INTEREST

None declared.

APPENDIX A. SUPPLEMENTARY DATA

Supplementary data to this article can be found online at https://doi.org/10.1016/j.molmet.2021.101326.

REFERENCES

[1] Ahmad, T.R., Haeusler, R.A., n.d. Bile acids in glucose metabolism and insulin signalling — mechanisms and research needs. Nature Reviews Endocrinology, Doi: 10.1038/s41574-019-0266-7.

[2] Li, T., Apte, U., 2015. Bile acid metabolism and signaling in cholestasis, inflammation, and cancer, 1st ed, vol. 74. Elsevier.

[3] Shin, D., Wang, L., 2019. Bile acid-activated Receptors : a review on FXR and other nuclear receptors. Springer Nature Switzerland.

[4] Kliewer, S.A., Mangelsdorf, D.J., 2015. Bile acids as hormones: the FXR-FGF15/19 pathway. Digestive Diseases 33(3):327—331. https://doi.org/10.1159/000371670.

[5] Chiang, J.Y.L., 2017. Bile acid metabolism and signaling in liver disease and therapy. Liver Research 1(1):3—9. https://doi.org/10.1016/j.livres.2017.05.001.

[6] Chen, L., van den Munckhof, I.C.L., Schraa, K., ter Horst, R., Koehorst, M., van Faassen, M., et al., 2020. Genetic and microbial associations to plasma and fecal bile acids in obesity relate to plasma lipids and liver fat content. Cell Reports 33(1):108212. https://doi.org/10.1016/j.celrep.2020.108212.

[7] Haeusler, R.A., Camastra, S., Nannipieri, M., Astiarraga, B., Castro-Perez, J., Xie, D., et al., 2016. Increased bile acid synthesis and impaired bile acid transport in human obesity. Journal of Clinical Endocrinology & Metabolism 101(5):1935—1944. https://doi.org/10.1210/jc.2015-2583.

[8] Haeusler, R.A., Astiarraga, B., Camastra, S., Accili, D., Ferrannini, E., 2013. Human insulin resistance is associated with increased plasma levels of 12a-hydroxylated bile acids. Diabetes 62(12):4184—4191. https://doi.org/10.2337/db13-0639.

[9] Sayin, S.I., Wahlström, A., Felin, J., Jäntti, S., Marschall, H.U., Bamberg, K., et al., 2013. Gut microbiota regulates bile acid metabolism by reducing the levels of tauro-beta-muricholic acid, a naturally occurring FXR antagonist. Cell Metabolism 17(2):225—235. https://doi.org/10.1016/j.cmet.2013.01.003.

[10] Hu, X., Bonde, Y., Eggertsen, G., Rudling, M., 2014. Muricholic bile acids are potent regulators of bile acid synthesis via a positive feedback mechanism. Journal of Internal Medicine 275(1):27—38. https://doi.org/10.1111/joim.12140.

[11] Li, F., Jiang, C., Krausz, K.W., Li, Y., Albert, I., Hao, H., et al., 2013. Microbiome remodelling leads to inhibition of intestinal farnesoid X receptor signalling and decreased obesity. Nature Communications 4(May). https://doi.org/10.1038/ncomms3384.

[12] Wang, D.Q.H., Tazuma, S., Cohen, D.E., Carey, M.C., 2003. Feeding natural hydrophilic bile acids inhibits intestinal cholesterol absorption: studies in the gallstone-susceptible mouse. American Journal of Physiology - Gastrointestinal and Liver Physiology 285(3 48—3):494—502. https://doi.org/10.1152/ajpgi.00156.2003.

[13] Li-hawkins, J., Gåfvels, M., Olin, M., Lund, E.G., Andersson, U., Schuster, G., et al., 2002. Cholic acid mediates negative feedback regulation 110(8):1191—1200. https://doi.org/10.1172/JCI200216309.Introduction. October.

[14] Kaur, A., Patankar, J.V., De Haan, W., Ruddle, P., Wijesekara, N., Groen, A.K., et al., 2015. Loss of Cyp8b1 improves glucose homeostasis by increasing GLP-1. Diabetes 64(4):1168—1179. https://doi.org/10.2337/db14-0716.

[15] Bonde, Y., Eggertsen, G., Rudling, M., 2016. Mice abundant in muricholic bile acids show resistance to dietary induced steatosis, weight gain, and to impaired glucose metabolism. PloS One 11(1). https://doi.org/10.1371/journal.pone.0147772.

[16] Bertaggia, E., Jensen, K.K., Castro-Perez, J., Xu, Y., Di Paolo, G., Chan, R.B., et al., 2017. Cyp8b1 ablation prevents Western diet-induced weight gain and hepatic steatosis because of impaired fat absorption. American Journal of Physiology - Endocrinology And Metabolism 313(2):E121—E133. https://doi.org/10.1152/ajpendo.00409.2016.

[17] Higuchi, S., Ahmad, T.R., Argueta, D.A., Perez, P.A., Zhao, C., Schwartz, G.J., et al., 2020. Bile acid composition regulates GPR119-dependent intestinal lipid sensing and food intake regulation in mice. Gut, 1—9. https://doi.org/10.1136/gutjnl-2019-319693.

[18] Takahashi, S., Fukami, T., Masuo, Y., Brocker, C.N., Xie, C., Krausz, K.W., et al., 2016. Cyp2c70 is responsible for the species difference in bile acid metabolism between mice and humans. Journal of Lipid Research 57(12):2130—2137. https://doi.org/10.1194/jlr.m071183.

[19] de Boer, J.F., Verkade, E., Mulder, N.L., de Vries, H.D., Huijkman, N., Koehorst, M., et al., 2020. A human-like bile acid pool induced by deletion of hepatic Cyp2c70 modulates effects of FXR activation in mice. Journal of Lipid Research 61(3):291—305. https://doi.org/10.1194/jlr.RA119000243.

[20] Honda, A., Miyazaki, T., Iwamoto, J., Hirayama, T., Morishita, Y., Monma, T., et al., 2020. Regulation of bile acid metabolism in mouse models with hydrophobic bile acid composition. Journal of Lipid Research 61(1):54—69. https://doi.org/10.1194/jlr.RA119000395.

[21] Straniero, S., Laskar, A., Savva, C., Härdfeldt, J., Angelin, B., Rudling, M., 2020. Of mice and men: murine bile acids explain species differences in the regulation of bile acid and cholesterol metabolism. Journal of Lipid Research 61(4):480—491. https://doi.org/10.1194/jlr.RA119000307.

[22] Scheer, N., Kapelyukh, Y., Chatham, L., Rode, A., Buechel, S., Wolf, C.R., 2012. Generation and characterization of novel cytochrome P450 Cyp2c gene cluster knockout and CYP2C9 humanized mouse lines. Molecular Pharmacology 82(6):1022—1029. https://doi.org/10.1124/mol.112.080036.

[23] Nelson, D.R., Zeldin, D.C., Hoffman, S.M.G., Maltais, L.J., Wain, H.M., Nebert, D.W., 2003. Comparison of cytochrome P450 (CYP) genes from the mouse and human genomes, including nomenclature recommendations for genes, pseudogenes and alternative-splice variants. Pharmacogenetics 450(1):1—18. https://doi.org/10.1097/01.fpc.0000054151.92680.31.

[24] Halldorsdottir, S., Carmody, J., Boozer, C.N., Leduc, C.A., Leibel, R.L., 2009. Reproducibility and accuracy of body composition assessments in mice by dual energy x-ray absorptiometry and time domain nuclear magnetic resonance. International Journal of Basic and Clinical Research 7(4):147—154.

[25] Mina, A.I., LeClair, R.A., LeClair, K.B., Cohen, D.E., Lantier, L., Banks, A.S., 2018. CalR: a web-based analysis tool for indirect calorimetry experiments. Cell Metabolism 28(4):656—666. https://doi.org/10.1016/j.cmet.2018.06.019 e1.

[26] Jones, R.D., Repa, J.J., Russell, D.W., Dietschy, J.M., Turley, S.D., 2012. Delineation of biochemical, molecular, and physiological changes accompanying bile acid pool size restoration in Cyp7a1 -/- mice fed low levels of cholic acid. American Journal of Physiology - Gastrointestinal and Liver Physiology 303(2). https://doi.org/10.1152/ajpgi.00111.2012.

[27] Keane, M.H., Overmars, H., Wikander, T.M., Ferdinandusse, S., Duran, M., Wanders, R.J.A., et al., 2007. Bile acid treatment alters hepatic disease and bile acid transport in peroxisome-deficient PEX2 Zellweger mice. Hepatology 45(4):982—997. https://doi.org/10.1002/hep.21532.

[28] Millar, J.S., Cromley, D.A., McCoy, M.G., Rader, D.J., Billheimer, J.T., 2005. Determining hepatic triglyceride production in mice: comparison of poloxamer 407 with Triton WR-1339. Journal of Lipid Research 46(9):2023—2028. https://doi.org/10.1194/jlr.D500019-JLR200.

[29] Jiao, S., Cole, T.G., Kitchens, R.T., Pfleger, B., Schonfeld, G., 1990. Genetic heterogeneity of lipoproteins in inbred strains of mice: analysis by gel-permeation chromatography. Metabolism 39(2):155—160. https://doi.org/10.1016/0026-0495(90)90069-0.

[30] Parlee, S.D., Lentz, S.I., Mori, H., MacDougald, O.A., 2014. Quantifying size and number of adipocytes in adipose tissue, 1st ed, vol. 537. Elsevier.

[31] de Boer, J.F., de Vries, H.D., Palmiotti, A., Li, R., Doestzada, M., Hoogerland, J.A., et al., 2021. Cholangiopathy and biliary fibrosis in Cyp2c70-

deficient mice are fully reversed by ursodeoxycholic acid. Cmgh 11(4):1045–1069. https://doi.org/10.1016/j.jcmgh.2020.12.004.

[32] Heuman, D.M., 1989. Quantitative estimation of the hydrophilic-hydrophobic balance of mixed bile salt solutions. Journal of Lipid Research 30(5):719–730. https://doi.org/10.1016/s0022-2275(20)38331-0.

[34] Weisberg, S.P., McCann, D., Desai, M., Rosenbaum, M., Leibel, R.L., Ferrante, A.W., 2003. Obesity is associated with macrophage accumulation in adipose tissue. Journal of Clinical Investigation 112(12):1796–1808. https://doi.org/10.1172/JCI200319246.

[35] De Victoria, E.O.M., Xu, X., Koska, J., Francisco, A.M., Scalise, M., Ferrante, A.W., et al., 2009. Macrophage content in subcutaneous adipose tissue: associations with adiposity, age, inflammatory markers, and whole-body insulin action in healthy pima Indians. Diabetes 58(2):385–393. https://doi.org/10.2337/db08-0536.

[36] Morgan, K., Uyuni, A., Nandgiri, G., Mao, L., Castaneda, L., Kathirvel, E., et al., 2008. Altered expression of transcription factors and genes regulating lipogenesis in liver and adipose tissue of mice with high fat diet-induced obesity and nonalcoholic fatty liver disease. European Journal of Gastroenterology and Hepatology 20(9):843–854. https://doi.org/10.1097/MEG.0b013e3282f9b203.

[37] Diraison, F., Dusserre, E., Vidal, H., Sothier, M., Beylot, M., 2002. Increased hepatic lipogenesis but decreased expression of lipogenic gene in adipose tissue in human obesity. American Journal of Physiology - Endocrinology And Metabolism 282(1 45–1):46–51. https://doi.org/10.1152/ajpendo.2002.282.1.e46.

[38] Song, P., Zhang, Y., Klaassen, C.D., 2011. Dose-response of five bile acids on serum and liver bile acid concentrations and hepatotoxicty in mice. Toxicological Sciences 123(2):359–367. https://doi.org/10.1093/toxsci/kfr177.

[39] Woolbright, B.L., Li, F., Xie, Y., Farhood, A., Fickert, P., Trauner, M., et al., 2014. Lithocholic acid feeding results in direct hepato-toxicity independent of neutrophil function in mice. Toxicology Letters 228(1):56–66. https://doi.org/10.1016/j.toxlet.2014.04.001.

[40] Oizumi, K., Sekine, S., Fukagai, M., Susukida, T., Ito, K., 2017. Identification of bile acids responsible for inhibiting the bile salt export pump, leading to bile acid accumulation and cell toxicity in rat hepatocytes. Journal of Pharmaceutical Sciences 106(9):2412–2419. https://doi.org/10.1016/j.xphs.2017.05.017.

[41] Corrigan, J.K., Ramachandran, D., He, Y., Palmer, C.J., Jurczak, M.J., Chen, R., et al., 2020. A big-data approach to understanding metabolic rate and response to obesity in laboratory mice. ELife 9:1–34. https://doi.org/10.7554/eLife.53560.

[42] Yao, L., Seaton, S.C., Ndousse-Fetter, S., Adhikari, A.A., Dibenedetto, N., Mina, A.I., et al., 2018. A selective gut bacterial bile salt hydrolase alters host metabolism. ELife 7:1–32. https://doi.org/10.7554/eLife.37001.

[43] Jiang, C., Xie, C., Lv, Y., Li, J., Krausz, K.W., Shi, J., et al., 2015. Intestine-selective farnesoid X receptor inhibition improves obesity-related metabolic dysfunction. Nature Communications 6:1–18. https://doi.org/10.1038/ncomms10166.

[44] Chen, Y., Goldstein, J.A., 2009. The transcriptional regulation of the human CYP2C genes Yuping. Current Drug Metabolism 10(6):567–578. https://doi.org/10.1038/jid.2014.371.

[45] Graves, J.P., Gruzdev, A., Bradbury, J.A., Degraff, L.M., Edin, M.L., Zeldin, D.C., 2017. Characterization of the tissue distribution of the mouse Cyp2c subfamily by quantitative PCR analysiss. Drug Metabolism and Disposition 45(7):807–816. https://doi.org/10.1124/dmd.117.075697.

